Electronic Supplementary Material (ESI) for Catalysis Science & Technology.

Supplementary Information: Halogenation as a Novel Scheme for Enhanced Photocatalytic Activity in AlSb Monolayer: A First-Principles Study

Rifat Shahriar[1], Khondker Shihabul Hoque [1], Ahmed Zubair[1,*]

[1]Department of Electrical and Electronic Engineering, Bangladesh
University of Engineering and Technology, Dhaka 1205, Bangladesh
*ahmedzubair@eee.buet.ac.bd

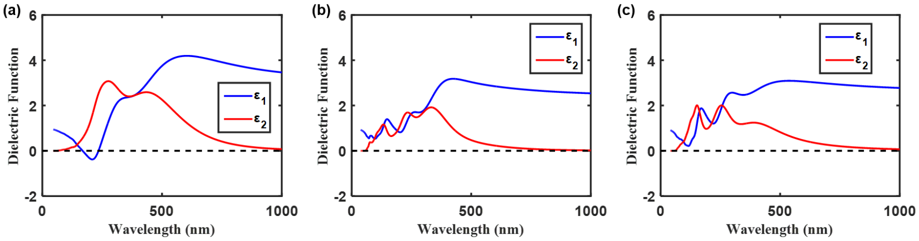

Figure S1: Dielectric functions of (a) pristine, (b) bromine doped, and (c) iodine dope AlSb monolayer.

S1 Calculation Details of Optical Properties

We calculated the absorption coefficient from the imaginary part of the complex dielectric function. The imaginary part of the dielectric function, ε_2, was calculated by summing over conduction bands by the method proposed in [1],

$$\varepsilon_2\left(\mathbf{q} \to O_{\hat{u}}, \hbar\omega\right) = \frac{2e^2\pi}{\Omega\varepsilon_0} \sum_{\mathbf{k},\nu,c} \left|\langle \Psi_{\mathbf{k}}^c | \mathbf{u}\cdot\mathbf{r} | \Psi_{\mathbf{k}}^\nu \rangle\right|^2 \delta\left(E_{\mathbf{k}}^c - E_{\mathbf{k}}^\nu - \hbar\omega\right), \tag{S1}$$

where $\mathbf{u}$ is the vector defining the polarization of the incident light, $|\langle \Psi_{\mathbf{k}}^c | \mathbf{u}\cdot\mathbf{r} | \Psi_{\mathbf{k}}^\nu \rangle|$ is the matrix element. $E_{\mathbf{k}}^c$ and $E_{\mathbf{k}}^v$ are the energy of the conduction band and valence band at wave number k, respectively. The charge of an electron is denoted by e, ω is the angular frequency, $\hbar$ is the reduced Planck's constant, $\mathbf{u.r}$ is the momentum operator, and Ω is the crystal volume. The real part, ε_1 was obtained using the Kramers-Kronig transformation given by [2],

$$\varepsilon_1(\omega) = 1 + \frac{2}{\pi} P \int_0^\infty \frac{\varepsilon_2\left(\omega^*\right)\omega^*}{\omega^{*2} - \omega^2} \mathrm{d}\omega^*. \tag{S2}$$

Here, P is the principal value of the integral. The complex refractive indices, n and κ, are related to the dielectric functions by the following equation:

$$\varepsilon_1(\omega) = n^2 - \kappa^2. \tag{S3}$$

$$\varepsilon_2(\omega) = 2n\kappa. \tag{S4}$$

The absorption coefficient, α is related to the imaginary and real dielectric constants by,

$$\alpha(\omega) = \frac{4\pi\kappa(\omega)}{\lambda} = \frac{4\pi}{\lambda\sqrt{2}} \left(\sqrt{\varepsilon_1^2(\omega) + \varepsilon_2^2(\omega)} - \varepsilon_1(\omega)\right)^{1/2}, \tag{S5}$$

where κ is the extinction coefficient and λ is the wavelength. The calculated complex dielectric functions for pristine, brominated, and iodinated AlSb monolayers are presented in Figs. S1(a-c).

S2 Orbital Projected Band Structure of Halogenated AlSb Monolayer

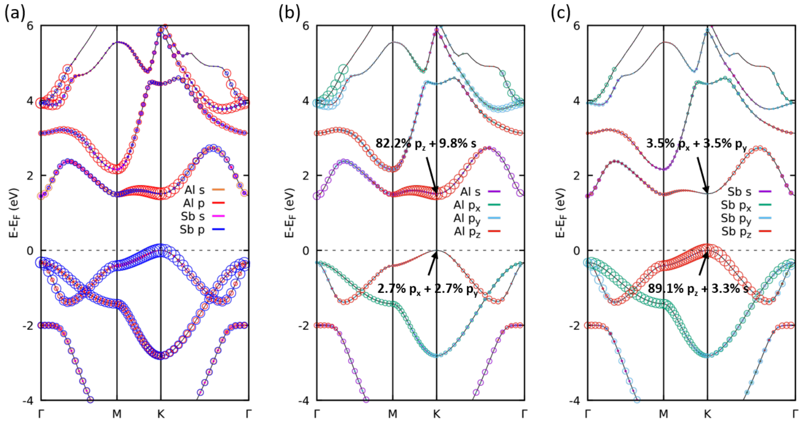

Figure S2: Orbital projected band diagram of AlSb monolayer showing the contribution of (a) Al, Sb atoms, (b) s and p orbitals of Al atom, and (c) s and p orbitals of Sb atom.

We performed projection of atomic orbitals on the band structure using quantum ESPRESSO [3] simulation package. To avoid computational complexity, orbital projections were performed without considering the hybrid functional. As a result, the band gaps were underestimated; however, the overall shape of the band structures remained unchanged which is sufficient for analyzing contributions from the atomic orbitals. Orbital projected band diagram of pristine AlSb monolayer is shown in Fig. S2. As can be seen from Fig. S2(a), Sb-p orbital contributions were pronounced in the valence band while Al-p orbital contributions were dominant in the conduction band. At valence band maxima (VBM), p_x and p_y orbitals of the Al atom contributed only 2.7% each, while the p_z orbital of the Sb atom contributed 89.1%. On the contrary, at conduction band minima (CBM), p_z orbital of the Al atom contributed 82.2% while p_x and p_y orbitals of the Sb atom only contributed 3.5% each.

Orbital projected band diagram of $AlSbF_2$ monolayer is shown in Figs. S3(a-d). The top valence band originated mostly from the p orbitals of Sb atoms while lower energy states inside the valence band originated from the p orbitals of F atoms. However, p_y (52.4%) and p_x (17.5%) orbitals of the Sb atom contributed mostly at VBM situated at Γ point. Moreover, p_y and p_x orbitals of F and Al atoms showed a smaller amount of contribution compared to the Sb atom at VBM. In contrast, p_z orbitals of the Al atom (37.9%) and the Sb atom (31.0%) dominated the contributions at CBM. However, contributions of F atomic orbitals were really small at CBM.

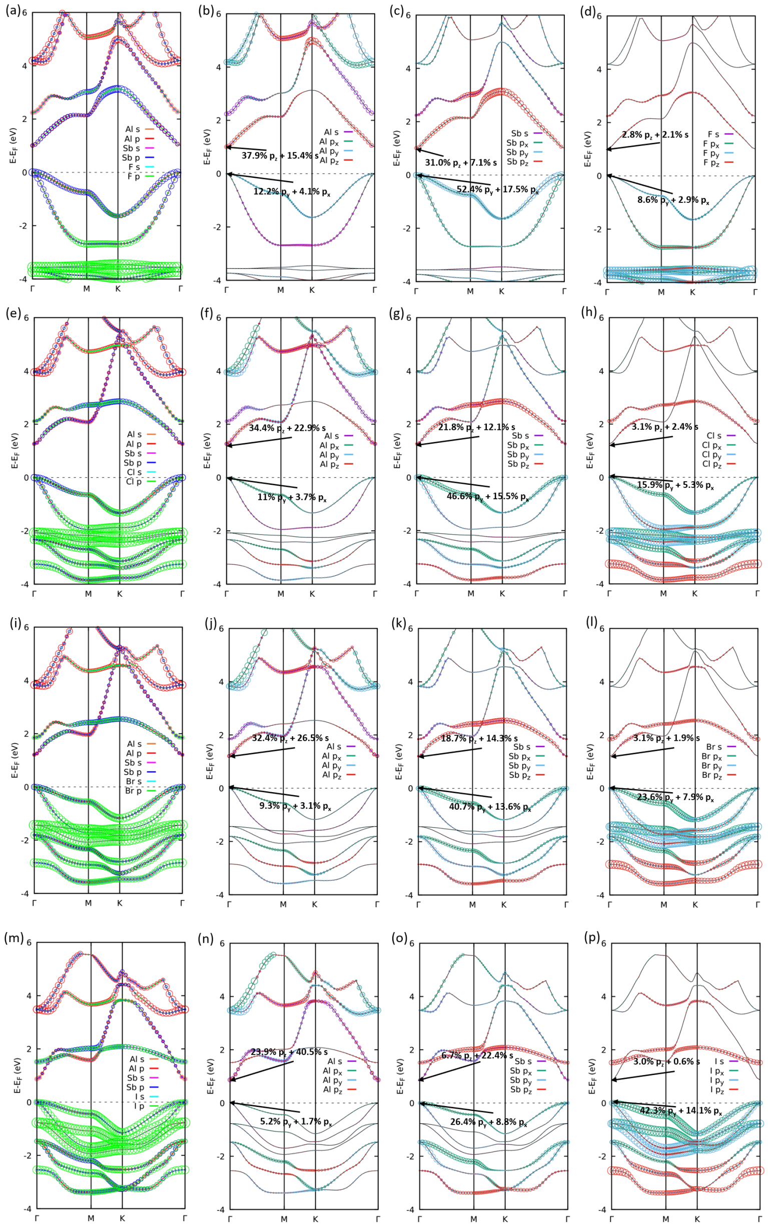

Figure S3: Orbital projected band diagram of $\mathrm{AlSbF_2}$ monolayer showing contributions of (a) Al, Sb, F atoms, (b) s, p orbitals of Al atom, (c) s, p orbitals of Sb atom, and (d) s, p orbitals of F atoms. $\mathrm{AlSbCl2_2}$ monolayer: (e) Al, Sb, Cl atoms, (f) s, p orbitals of Al atom, (g) s, p orbitals of Sb atom, and (h) s, p orbitals of Cl atoms. $\mathrm{AlSbBr_2}$ monolayer: (i) Al, Sb, Br atoms, (j) s, p orbitals of Al atom, (k) s, p orbitals of Sb atom, and (l) s, p orbitals of Br atoms. $\mathrm{AlSbI_2}$ monolayer: (m) Al, Sb, I atoms, (n) s, p orbitals of Al atom, (o) s, p orbitals of Sb atom, and (p) s, p orbitals of I atoms.

Orbital projected band diagram of $AlSbCl_2$ monolayer is shown in Figs. S3(e-h). In the valence band, states originated mostly from the p orbitals of Cl atoms. However, p_y (46.6%) and p_x (15.5%) orbitals of the Sb atom contributed mostly at VBM situated at Γ point. Moreover, p_y and p_x orbitals of Cl and Al atoms showed a smaller amount of contribution compared to the Sb atom at VBM. In contrast, p_z (34.4%) and s (22.9%) orbitals of the Al atom dominated the contributions at CBM. Additionally, p_z (21.8%) and s (12.1%) orbitals of the Sb atom showed comparable contributions. However, contributions of Cl atomic orbitals were really small at CBM.

Orbital projected band diagram of $AlSbBr_2$ monolayer is shown in Figs. S3(i-l). In the valence band, states originated mostly from the p orbitals of Br atoms. Similar to the previous case, p_y (40.7%) and p_x (13.6%) orbitals of Sb atoms contributed mostly at VBM situated at Γ point though the amount of contribution decreased compared to $AlSbCl_2$. On the other hand, p_y (23.6%) and p_x (7.9%) orbitals of Br atoms contributed more at VBM compared to Cl atoms in the previous case. Consequently, p_y and p_x orbital contributions of the Al atom reduced further at VBM. At CBM, p_z (32.4%) and s (26.5%) orbitals of the Al atom dominated the contributions. Moreover, p_z (18.7%) and s (14.3%) orbitals of the Sb atom also showed comparable contributions. However, contributions of Br atomic orbitals were really small at CBM, similar to $AlSbCl_2$.

Orbital projected band diagram of $AlSbI_2$ monolayer is shown in Figs. S3(m-p). Similar to the previous two cases, p orbitals of I atoms dominated the valance band states. In contrast to $AlSbCl_2$ and $AlSbBr_2$, p_y (42.3%) and p_x (14.1%) orbitals of I atoms dominated the VBM at Γ point. Moreover, p_y and p_x orbitals of the Sb atom contributed 26.4% and 8.8% respectively, which were low compared to the previous cases. At CBM, s orbital (40.5%) of the Al atom contributed more than the p_z orbital (23.9%) of the Al atom in contrast with the previous cases. Similarly, the s orbital of the Sb atom contributed more than its p_z orbital. Atomic orbital contributions of I atoms at CBM were small, similar to the previous cases.

Apart from the fully halogenated AlSb monolayer, the partially halogenated AlSb monolayer was also exploited. A representative structure of a partially halogenated AlSb monolayer is presented in Fig. S4(a). However, these structures were found to be metallic as can be seen in Figs. S4(b-d). The valence band maxima are pulled upwards into the conduction band, which leads to a zero bandgap electronic structure. The metallicity could have been caused by a multitude of reasons. For instance, the asymmetry in the structure, and the delocalized electrons could have caused the metallicity. Furthermore, the halogen dopants are highly electronegative which could have caused the bands to shift. Compared to the pristine structure, new states originated in the valence band that penetrated the conduction band.

To understand the origin of the band structure modification, we calculated and compared the band structures projected onto atomic orbitals of Al, Sb, and X (halogen) atoms for pristine AlSb, fully halogen decorated AlSb, and partially halogen decorated AlSb. The **E-k** band structures and orbital projected band

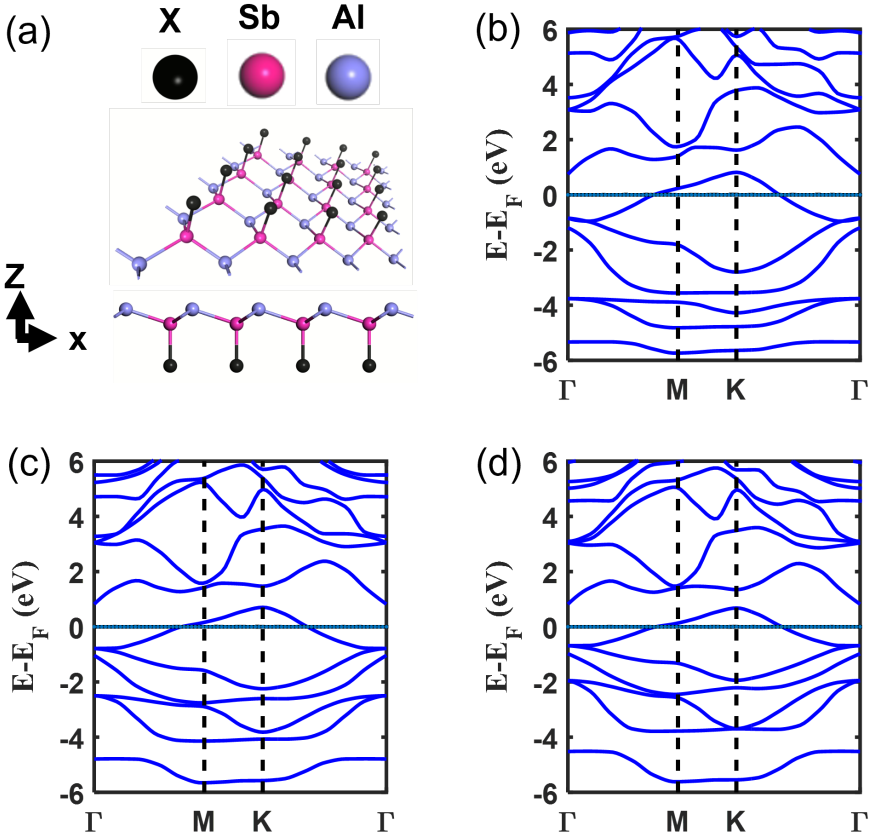

Figure S4: (a) Perspective and side views of a partially halogenated AlSb monolayer. Band structures of (b) AlSbF, (c) AlSbCl, and (d) AlSbBr monolayers.

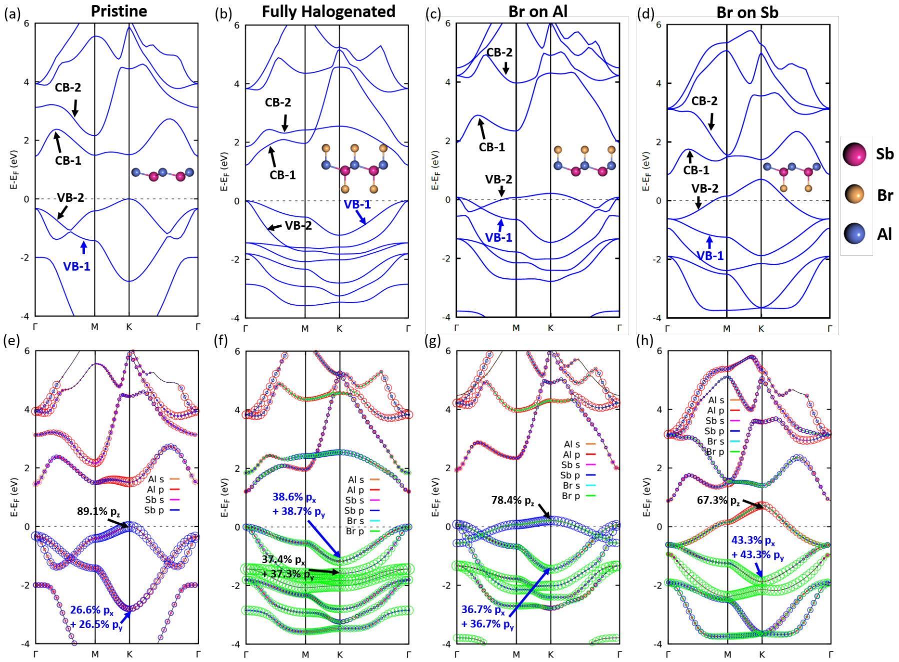

Figure S5: Band diagram of (a) pristine AlSb, (b) fully Br decorated AlSb, (c) Partially Br decorated (on Al) AlSb, and (d) Partially Br decorated (on Sb) AlSb monolayer calculated using PBE. The top two valence bands and the bottom two conduction bands are marked in each case. Orbital projected band diagram of (e) pristine AlSb, (f) fully Br decorated AlSb, (g) Partially Br decorated AlSb (on Al), and (h) Partially Br decorated AlSb (on Sb) monolayers.

diagram of pristine AlSb and Br decorated AlSb are shown in Fig. S5. Moreover, we calculated Mulliken charge transfer for fully and partially Br decorated cases as shown in Table S1. Although the top valence band (VB-2) states increased in energy with the increase of **k** value in the pristine case, the same band decreased in energy with the increase of **k** magnitude in the fully halogenated case. For partial halogenation, the same trend of parabolic increase of the top valence band was seen with **k** value similar to the pristine case; however, the band crossed the Fermi level because of the change in charge transfer and orbital contributions.

In a pristine AlSb monolayer, it is clear that electrons transferred from Al to Sb atoms from the Mulliken charge transfer calculations. Consequently, filled states in the valence band top originated from Sb p orbitals, and empty states in the conduction band bottom came from Al p orbitals (See Fig. S5). From the orbital contribution, it was seen that states in the top valence band (VB-2) at **K** point originated mostly from bonding p_π (i.e., p_z orbitals) of Sb atoms (see Fig. S5(e)). As a result, the band exhibited an increasing trend with the increase

Table S1: Mulliken Charge Transfer for Br Decoration

Structure	$Q_{Al}(\lvert e\rvert)$	$Q_{Sb}(\lvert e\rvert)$	$Q_{X-Al}(\lvert e\rvert)$	$Q_{X-Sb}(\lvert e\rvert)$
AlSb	0.21	-0.21	–	–
$AlSbBr_2$	0.35	0.30	-0.35	-0.30
AlSbBr (on Al)	0.39	-0.10	-0.29	–
AlSbBr (on Sb)	0.11	0.17	–	-0.28

of **k** value and the maximum was at K point which has the highest magnitude of **k** in the k-path presented in the figure. In contrast, VB-1 originated mostly from p_σ-based orbitals (p_x and p_y) of Sb and Al atoms which gave the band a parabolic decrease with the increase of **k** value.

When the AlSb monolayer was fully Br decorated, charge transferred from both Al and Sb atoms to Br atoms. As a result, valence band states originated primarily from Br p orbitals. Moreover, from the orbital contribution, it was seen that states at VB-2 were mostly generated from p_x and p_y orbitals (see Fig. S5(f)) rather than s or p_z orbitals compared to the pristine case. As a result, VB-2 underwent a decrease with the increase of **k** value and consequently, VBM was shifted from K point to Γ point.

When AlSb was partially halogenated by functionalizing only the Al atoms with Br, charge transferred from Al atoms to both Sb atoms and Br atoms. However, charge transfer to Sb atoms was less compared to the pristine case. As a result, VB-2 crossed the Fermi level because of the empty states in Sb atoms due to less electron transfer. From the orbital contributions, it was seen that states in VB-2 at K point originated mostly from p_z orbitals of Sb atoms (see Fig. S5). Consequently, the band exhibited a parabolic increase with the increase of **k** value and the maximum was at K point similar to the pristine case. Finally, When AlSb was partially halogenated by functionalizing only the Sb atoms with Br, charge transferred from Al and Sb atoms to Br atoms. However, the amount of charge transfer from Al atoms was less compared to the previous three cases. As a result, the top of VB-2 mostly originated from Al-p orbitals, and consequently, the band crossed the Fermi level. Moreover, states at K point in VB-2 originated mostly from p_z orbitals of Al atoms, resulting in a parabolic increase of energy values with the increase of **k** values (see Fig. S5(h)).

In summary, only when the AlSb monolayer was fully halogenated, the VB-2 valence band originated from pσ-based orbitals resulting in curvature reversal and downward shift of the band. Consequently, VBM shifted from **K** point to Γ point. As a result, the bandgap increased in case of fully halogenated $AlSbCl_2$ and $AlSbBr_2$ monolayers compared to the pristine case.

Projection of different atomic orbitals on the band diagram and projected density of states are shown in Fig. S6 and Fig. S7 for partial Br decoration on Al atoms and on Sb atoms respectively. As discussed earlier, when only Al atoms were functionalized by Br, top valence band originated mostly from p_z orbitals of Sb atoms. On the other hand, top valence band originated mostly from p_z orbitals of Al atoms when only Sb atoms were functionalized by Br.

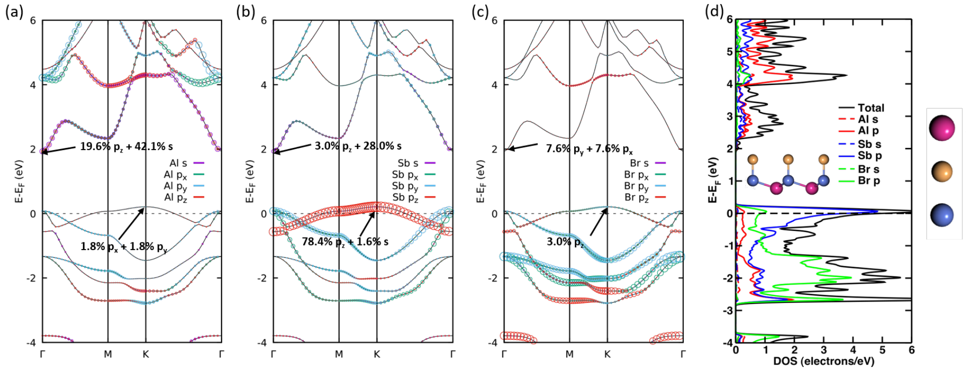

Figure S6: Orbital projected band diagram of partially Br decorated (on Al) AlSb monolayer showing the contribution of (a) s and p orbitals of Al atom, (b) s and p orbitals of Sb atom, and (c) s and p orbitals of Br atom. (d) Projected DOS of partially Br decorated (on Al) AlSb monolayer.

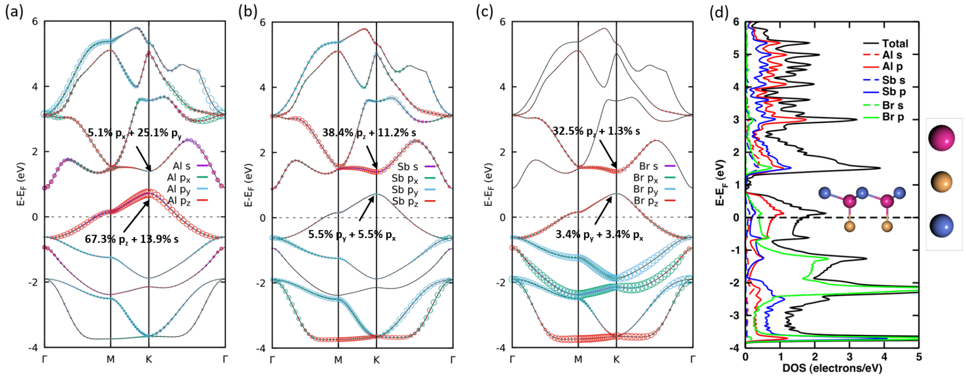

Figure S7: Orbital projected band diagram of partially Br decorated (on Sb) AlSb monolayer showing the contribution of (a) s and p orbitals of Al atom, (b) s and p orbitals of Sb atom, and (c) s and p orbitals of Br atom. (d) Projected DOS of partially Br decorated (on Sb) AlSb monolayer.

S3 Calculation Method of Electronegativity

We calculated the Mulliken electronegativity of $AlSbX_2$ by calculating the geometric mean of the Mulliken electronegativity of the constituent atoms. Mulliken electronegativity, χ of an atom can be expressed by,

$$\chi = (E_i + E_a)/2. \tag{S6}$$

Here, E_i and E_a are the ionization energy and electron affinity, respectively. The calculated electronegativity of F, Cl, Br, I, Al, and Sb atoms are shown in Table S2. The electronegativity of $AlSbX_2$ is calculated by,

$$\chi_{AlSbX_2} = (\chi_{Al} \times \chi_{Sb} \times \chi_X \times \chi_X)^{1/4}. \tag{S7}$$

Table S2: Mulliken electronegativity of F, Cl, Br, I, Al, and Sb

Atom	E_i (eV)	E_a (eV)	χ (eV)
F	17.42	3.40	10.41
Cl	12.97	3.60	8.29
Br	11.81	3.36	7.59
I	10.45	3.06	6.75
Al	5.98	0.43	3.21
Sb	9.00	1.05	4.85

S4 Calculation Method of Gibbs Free Energy

The method for calculation of Gibbs free energy is discussed briefly in Section 2 (Methods) of the main manuscript. In the OER reaction, the free energy difference between the consecutive steps can be written as,

$$\Delta G_1 = G^*_{OH} + \frac{1}{2}G_{H_2} - G^* - G_{H_2O} + \Delta G_U + \Delta G_{pH} \tag{S8}$$

$$\Delta G_2 = G^*_O + \frac{1}{2}G_{H_2} - G_{OH^*} + \Delta G_U + \Delta G_{pH} \tag{S9}$$

$$\Delta G_3 = G^*_{OOH} + \frac{1}{2}G_{H_2} - G_{O^*} - G_{H_2O} + \Delta G_U + \Delta G_{pH} \tag{S10}$$

$$\Delta G_4 = G^* + \frac{1}{2}G_{H_2} + G_{O_2} - G_{OOH^*} + \Delta G_U + \Delta G_{pH} \tag{S11}$$

In HER, the energy difference in the consecutive steps are expressed as follows,

$$\Delta G_5 = GH^* - \frac{1}{2}G_{H_2} - G^* + \Delta G_U + \Delta G_{pH} \tag{S12}$$

$$\Delta G_6 = GH^* + \frac{1}{2}G_{H_2} - G_{H^*} + \Delta G_U + \Delta G_{pH} \tag{S13}$$

S5 Calculation Method of Solar to Hydrogen (STH) Efficiency

In order to explore the water-splitting efficiency of the halogen-decorated monolayers, we calculated the solar-to-hydrogen efficiency (η_{sth}). For the monolayers, the η_{sth} can be obtained by $\eta_{sth} = \eta_{abs} \times \eta_{cu}$ in this work. The η_{abs} and η_{cu} are the efficiency of light absorption and carrier utilization, respectively. Furthermore, the η_{abs} is described as:

$$\eta_{abs} = \frac{\int_{E_g}^{\infty} P\left(h\omega\right) d\left(h\omega\right)}{\int_{0}^{\infty} P\left(h\omega\right) d\left(h\omega\right)} \tag{S14}$$

where E_g is the band gap and $P\left(h\omega\right)$ is the AM1.5G solar flux at photon energy $h\omega$. The efficiency of carrier utilization as described below,

$$\eta_{cu} = \frac{\Delta G \int_{E}^{\infty} \frac{P(h\omega)}{h\omega} d\left(h\omega\right)}{\int_{E_g}^{\infty} P\left(h\omega\right) d\left(h\omega\right)} \tag{S15}$$

where the ΔG (1.23 eV) is the difference of the reduction and oxidation potentials for water splitting and the E represents the minimum photon energy that can participate in the redox reactions, described as:

$$E = \begin{array}{c} E_g, \left(\chi\left(H_2\right) \geq 0.2, \chi\left(O_2\right) \geq 0.6\right) \\ E_g + 0.2 - \chi\left(H_2\right), \left(\chi\left(H_2\right) < 0.2, \chi\left(O_2\right) \geq 0.6\right) \\ E_g + 0.6 - \chi\left(O_2\right), \left(\chi\left(H_2\right) \geq 0.2, \chi\left(O_2\right) < 0.6\right) \\ E_g + 0.8 - \chi\left(H_2\right) - \chi\left(O_2\right), \left(\chi\left(H_2\right) < 0.2, \chi\left(O_2\right) < 0.6\right) \end{array}$$

The $\chi\left(H_2\right)$ and $\chi\left(O_2\right)$ represent the overpotentials of the hydrogen and oxygen evolution reactions.

S6 Gibbs Free Energy Profile of OER and HER in Pristine AlSb Monolayer

The Gibbs free energy profiles of OER and HER in pristine AlSb monolayer are presented in Fig. S8. Contrary to the halogenated AlSb monolayer, the energy barrier here is positive. Hence, it can be concluded that halogen functionalization is responsible for the negative Gibbs free energy profile.

S7 Bandgap of bulk AlSb

The bandgap of bulk AlSb is presented in Fig. S9. The calculated bandgap was 1.634 eV which is in excellent agreement with the experimentally determined bandgap of 1.6 eV.

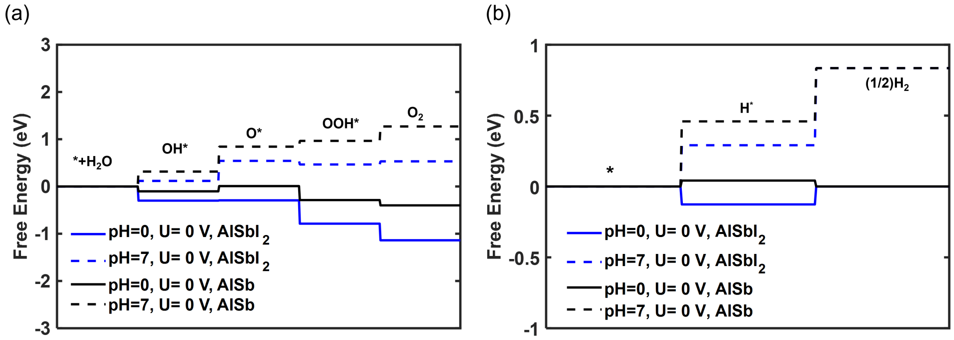

Figure S8: (a) OER and (b) HER reaction Gibbs free energy profile in pristine and halogenated AlSb monolayer.

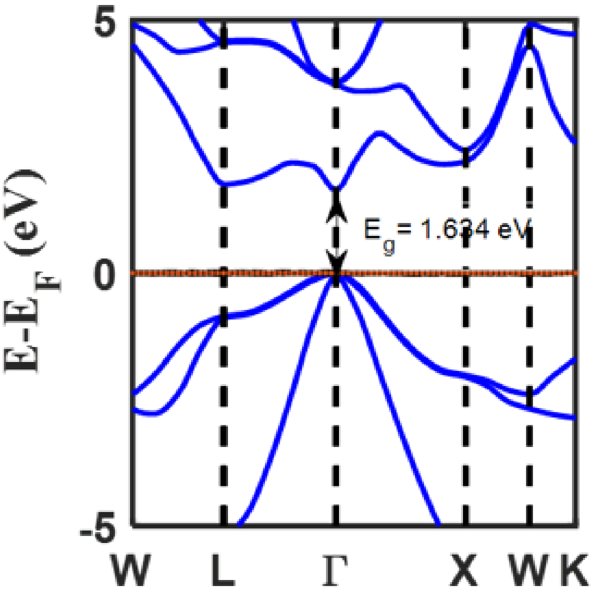

Figure S9: Bandgap of bulk AlSb

References

[1] M. Gajdoš, K. Hummer, G. Kresse, J. Furthmüller and F. Bechstedt, *Physical Review B*, 2006, **73**, 045112.

[2] E. D. Palik, *Handbook of Optical Constants of Solids*, 2012, **1**, 1–804.

[3] P. Giannozzi, S. Baroni, N. Bonini, M. Calandra, R. Car, C. Cavazzoni, D. Ceresoli, G. L. Chiarotti, M. Cococcioni, I. Dabo, A. Dal Corso, S. de Gironcoli, S. Fabris, G. Fratesi, R. Gebauer, U. Gerstmann, C. Gougoussis, A. Kokalj, M. Lazzeri, L. Martin-Samos, N. Marzari, F. Mauri, R. Mazzarello, S. Paolini, A. Pasquarello, L. Paulatto, C. Sbraccia, S. Scandolo, G. Sclauzero, A. P. Seitsonen, A. Smogunov, P. Umari and R. M. Wentzcovitch, *J. Phys.: Condens. Matter*, 2009, **21**, 395502 (19pp).